Sebastian Jäger*, Stephan Dickgiesser, Jason Tonillo, Stefan Hecht, Harald Kolmar and Christian Schröter*

EGFR binding Fc domain-drug conjugates: stable and highly potent cytotoxic molecules mediate selective cell killing

https://doi.org/10.1515/hsz-2021-0321
Received July 13, 2021; accepted September 7, 2021; published online September 20, 2021

Abstract: The exposition of cancer cells to cytotoxic doses of payload is fundamental for the therapeutic efficacy of antibody drug conjugates (ADCs) in solid cancers. To maximize payload exposure, tissue penetration can be increased by utilizing smaller-sized drug conjugates which distribute deeper into the tumor. Our group recently explored small human epidermal growth factor receptor 2 (HER2) targeting Fc antigen binding fragments (Fcabs) for ADC applications in a feasibility study. Here, we expand this concept using epidermal growth factor receptor (EGFR) targeting Fcabs for the generation of site-specific auristatin-based drug conjugates. In contrast to HER2-targeting Fcabs, we identified novel conjugation sites in the EGFR-targeting Fcab scaffold that allowed for higher DAR enzymatic conjugation. We demonstrate feasibility of resultant EGFR-targeting Fcab-drug conjugates that retain binding to half-life prolonging neonatal Fc receptor (FcRn) and EGFR and show high serum stability as well as target receptor mediated cell killing at sub-nanomolar concentrations. Our results emphasize the applicability of the Fcab format for the generation of drug conjugates designed for increased penetration of solid tumors and potential FcRn-driven antibody-like pharmacokinetics.

***Corresponding authors: Sebastian Jäger**, ADCs & Targeted NBE Therapeutics, Merck KGaA, Frankfurter Str. 250, D-64293 Darmstadt, Germany; and Institute for Organic Chemistry and Biochemistry, Technical University of Darmstadt, Alarich-Weiss-Str. 4, D-64287 Darmstadt, Germany, E-mail: sebastian.jaeger@merckgroup.com. https://orcid.org/0000-0002-1381-2759; and **Christian Schröter**, ADCs & Targeted NBE Therapeutics, Merck KGaA, Frankfurter Str. 250, D-64293 Darmstadt, Germany,
E-mail: christian.a.schroeter@merckgroup.com
Stephan Dickgiesser, Jason Tonillo and Stefan Hecht, ADCs & Targeted NBE Therapeutics, Merck KGaA, Frankfurter Str. 250, D-64293 Darmstadt, Germany
Harald Kolmar, Institute for Organic Chemistry and Biochemistry, Technical University of Darmstadt, Alarich-Weiss-Str. 4, D-64287 Darmstadt, Germany

Keywords: antibody-drug conjugates; antibody engineering; drug delivery; Fc antigen binding fragments; transglutaminase; tumor penetration.

Introduction

The field of antibody-drug conjugate (ADC) has recently attracted attention with the approval of six new ADCs between 2019 and April 2021 suggesting that excessive research on this class of cancer therapeutics is finally bearing fruit (Boni et al. 2020; Mullard 2020, 2021; Syed 2020). ADCs consist of cytotoxic drugs covalently linked to monoclonal antibodies allowing for selective surface receptor binding on cancer cells followed by delivery of the drug into the intracellular compartment (Khongorzul et al. 2020). Beside conventional ADCs generated from full-length 150 kDa monoclonal antibodies (mAbs), smaller antibody-fragment based drug conjugates designed for enhanced tumor penetration and efficacy have been explored (Aubrey et al. 2018; Cao et al. 2020; Deonarain 2018; Glassman et al. 2020; Higgins et al. 2020; Liu et al. 2019; Nessler et al. 2020; Q. Li et al. 2019; Ruddle et al. 2019).

In this regard, we have recently described antigen binding Fc fragments (Fcabs) as a promising format for the generation of drug conjugates (Jäger et al. 2021). Fcabs are derived from the Fc fragment of human IgG1 antibodies by engineering the C-terminal structural loops of the C_H3 domain to form an antigen binding site (Figure 1A, B). Hence, Fcabs combine Fc-mediated effector functions including neonatal Fc receptor (FcRn) binding with an antigen binding functionality but comprise only one third of the size of conventional IgGs (Lobner et al. 2016). The smaller size of the Fcab format promises to improve solid tumor penetration by enhancing the extravasation from the circulation into the interstitial space and increasing diffusion rates through the interstitium and tumor tissue (Thurber et al. 2008). Moreover, the half-life extending FcRn binding site delays systemic clearance of the Fcab (mouse terminal $t_{1/2}$ Fcab 60–85 h (Leung et al. 2015; Wozniak-Knopp et al. 2010)) and thereby maintains a high plasma concentration that further drives penetration into

tissues (Thurber et al., 2008). FcRn binding provides Fcabs with a significant advantage over other reported ≤50 kDa Fab- (Liu et al. 2019; Ruddle et al. 2019), scFv- (Aubrey et al. 2018; Higgins et al. 2020), diabody- (Q. Li et al. 2019) or single domain antibody-based drug conjugates (Cao et al. 2020; Glassman et al. 2020; Nessler et al. 2020) that lack an FcRn binding site and consequently suffer from a short half-life *in vivo* (mouse terminal $t_{1/2}$ Trastuzumab-derived Fab 4.4 h (Z. Li et al. 2019)). In our initial feasibility study, we were able to show that the Fcab format is suitable to generate HER2 binding drug conjugates. Deploying an engineered microbial transglutaminase, we were able to site-specifically conjugate linker-payloads to the conserved Fc position Q295 resulting in stable and functional Fcab-drug conjugates with a drug-to-antibody ratio (DAR) of 2.0. Furthermore, we demonstrated in an *in vitro* spheroid experiment, that spheroid accumulation was higher for Fcabs compared to full-length antibody controls confirming the favorable penetration capability of Fcabs (Jäger et al. 2021).

In the present study, we expand the concept of Fcab-based ADCs from HER2 to EGFR binding Fcab-ADCs and demonstrate the versatility of this antibody format for the generation of site-specific, stable and highly potent drug conjugates. We first demonstrate that the selected EGFR binding Fcabs are suitable for an ADC approach based on selective cellular uptake data using heterogenous conjugates carrying a pH dependent fluorescent dye. We then employed site-specific enzymatic conjugation to attach the microtubule inhibitor monomethyl auristatin E (MMAE) to position Q295 but also to the novel position Q311 and Q438 allowing to reach higher DARs. The drug conjugates showed retained EGFR and FcRn binding properties and possessed excellent stability in mouse and human serum. Finally, we show EGFR-mediated sub-nanomolar cytotoxicity of our Fcab-drug conjugates on different cancer cell lines.

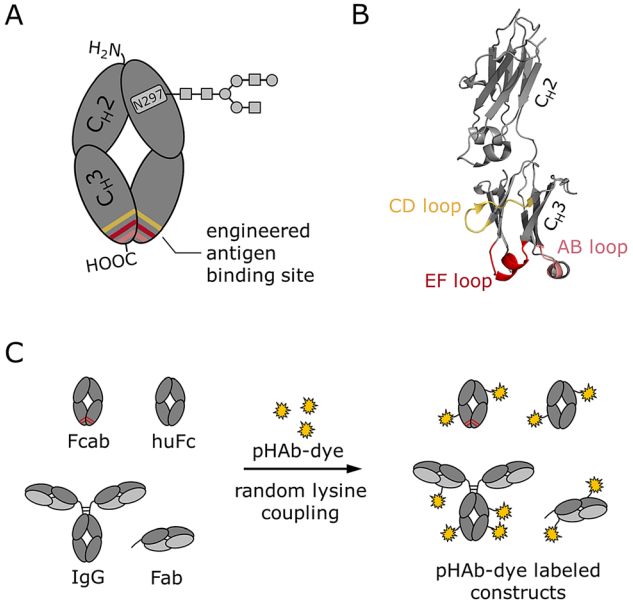

Figure 1: Fcab structure and pHAb-dye labeling.
(A) Schematic representation of homodimeric Fcab with engineered antigen binding site at the C-terminus of the C_H3 domain. (B) Human IgG1-Fc monomer depicting the C_H3 AB, CD and EF loops that were engineered in the selected EGFR-binding Fcabs (PDB ID 5JII). Glycosylation is not shown for clarity. (C) Schematic representation of pHAb-dye labeling.

Materials and methods

Preparation of antibody fragments

Amino acid sequences of Fcabs were taken from literature (Tuna et al. 2018). Sequences of Fcabs (no core hinge region, D265A) are given along with huFc (D265A) and Cetuximab sequences (SrtA tag) in the SI. Encoding sequences were ordered as codon-optimized versions and cloned into pTT5 vector for mammalian expression (GeneArt, Thermo Fisher Scientific). Fcabs and huFc controls were expressed by transient transfection of Expi293F™ cells following the manufacturer's instructions and the supernatants were harvested after five days post transfection. C-Fab contained a His_6-Tag for purification and was dialyzed against phosphate-buffered saline (PBS) pH 7.4 before purification by immobilized metal affinity chromatography (1 mL HisTrap™ HP, GE Healthcare) using an ÄKTA Pure device (GE Healthcare). Fcabs, huFc and C-IgG were purified by protein A affinity chromatography using HiTrap™ Mab Select SuRe 5 mL columns (GE Healthcare) and subsequently formulated in PBS pH 6.8 using HiPrep™ 26/10 desalting columns. Antibody purity was analyzed by analytical size exclusion (SE) HPLC using a TSKgel® SuperSW3000 column (Tosoh Bioscience) and by SDS gel electrophoresis. Identity of proteins was confirmed *via* intact mass analysis by LC-MS using an Exion LC and TripleTOF® 6600+ mass spectrometer (AB Sciex). Proteins were concentrated using Ultra centrifugal filter units (3 K MWCO, Amicon®), sterile filtered and protein concentration was determined by UV–VIS spectroscopy at 280 nm. Proteins were snap-frozen in liquid nitrogen and stored at −80 °C.

Preparation of MMAE conjugates

Fcabs and huFc were conjugated to drug-linker Gly_3-Val-Cit-PAB-MMAE (**1**, Levena) using a genetically engineered mTG (Dickgiesser et al. 2020). mTG-mediated antibody conjugation was performed using 5 mg/mL Fcabs/huFc, 20 molar equivalents of drug-linker and 60 U/mL mTG in PBS pH 6.8 with up to 10% DMSO. Reaction mixes were incubated at 37 °C for 18 h with gentle shaking, chilled to 10 °C and purified by preparative size exclusion chromatography (SEC).

For SrtA conjugation, C-IgG or C-Fab (5 mg/mL) were formulated in 150 mM NaCl, 50 mM Tris-HCl, 5 mM $CaCl_2$ pH 7.5. SrtA (Chen et al. 2011) was added to a final concentration of 13 μM along with 10

equivalents of Gly_3-Val-Cit-PAB-MMAE (**1**) per SrtA recognition motif. The reaction mixture was incubated for 90 min at 25 °C, stopped by the addition of EDTA (final 10 mM) and purified by preparative SEC.

Preparative SEC was performed using either a Superdex™ 200 Increase 10/300 GL, Superdex™ 75 10/30 GL or a Superdex™ 200 prep grade 16/60 column in a 1260 liquid chromatography system (Agilent Technologies) or an ÄKTA Avant device (GE Healthcare) with PBS pH 6.8 as running buffer. Purified conjugates were concentrated using Ultra centrifugal filter units (10 K MWCO, Amicon®), sterile filtered and protein concentration was determined by UV–VIS spectroscopy at 280 nm. The purified conjugates were subjected to analysis by SE-HPLC and DAR determination (reversed phase (RP) HPLC, LC-MS) as described elsewhere (Dickgiesser et al. 2020), snap-frozen in liquid nitrogen and stored at −80 °C.

Preparation of pHAb-dye conjugates

Fcabs, huFc and Cetuximab controls were formulated in 10 mM sodium-bicarbonate buffer pH 8.5. pHAb amine reactive dye (10 mg/mL 1:1 (v/v) DMSO/H_2O, Promega) was either added at a 2:1 molar ratio (pHAb:antibody) (Fcab-1, Fcab-2, Fcab-3, C-IgG, C-Fab) or a 10:1 molar ratio (huFc), followed by incubation at 25 °C, 450 rpm for 1 h in the absence of light. Excess dye was removed by Dulbecco's phosphate buffered saline (DPBS) equilibrated Zeba™ Spin desalting columns (ThermoFisher Scientific) according to the manufacturer's instructions. Aggregation of pHAb-dye conjugates and fluorescence degree of labeling (DOL^F) were determined by an SE-HPLC method described in the SI.

Peptide mapping

Fcab-1 and Fcab-1-MMAE were deglycosylated with GlycINATOR (Genovis) according to the instruction manual. Deglycosylated molecules were then reduced with 10 mM dithiothreitol (DTT) for 30 min at 56 °C and alkylated with 55 mM iodoacetamide for 30 min at room temperature in the dark. Ten microgram protein was digested with 0.5 µg trypsin (mass spectrometry grade, Promega) at 37 °C overnight.

LC-MS analysis was performed using an Exion HPLC system coupled to a TripleTOF 6600+ mass spectrometer (Sciex). 7.5 µg peptide solution was loaded onto an Aeris PEPTIDE XB-C18 column (Phenomenex, part no. 00F-4506-AN) and eluted with a linear gradient from 5 to 50% buffer B (acetonitrile, 0.1% formic acid; buffer A: water, 0.1% formic acid) within 49 min. Data were acquired with positive polarity and in a TOF-MS mass range from 350 to 2500 m/z and a TOF-MS/MS mass range from 50 to 2500 m/z. Other instrument settings were as follows: ion spray voltage 5.5 kV, source temperature 450 °C, accumulation time 0.25 s for TOF-MS and 0.08 s for TOF-MS/MS, gas1 45 psi, gas2 45 psi, curtain gas 35 psi, declustering potential 80 V, and collision energy was set to dynamic. Data were processed with Genedata Expressionist.

Cell culture

Human cancer cell lines were obtained from the American Type Culture Collection (EGFR positive: MDA-MB-468, A431; EGFR negative: MCF-7) and maintained according to standard culture conditions (37 °C, 5% CO_2, 95% humidity). A431 and MCF-7 cells were cultured in Dulbecco's modified Eagle's (DMEM) high glucose medium supplemented with 10% fetal bovine serum (FBS), 2 mM L-glutamine and 1 mM sodium pyruvate. MDA-MBA-468 cells were cultured in Roswell Park Memorial Institute (RPMI) 1640 medium supplemented with 10% FBS, 2 mM L-glutamine and 1 mM sodium pyruvate. For subculturing, adherent grown cells were detached by adding 0.05% trypsin-EDTA, diluted with fresh medium and transferred into a new culturing flask.

Cellular uptake

Cells were centrifuged at 500 × g for 5 min, the supernatant was discarded, and cells were resuspended in the respective medium without phenol red at 300,000 cells/mL. The cell suspension (40 µL/well) was seeded into a black 384 clear bottom plate followed by incubation (37 °C, 5% CO_2) in a humid chamber overnight. pHAb-dye labeled proteins were supplemented with 0.3% Tween-20 (final), diluted to 3 µM and added to the cells in triplicates (final 100 nM) using a D300e digital dispenser (Tecan). The cells were immediately transferred to a Cytation 5 cell imaging reader (BioTek) equipped with DAPI and RFP filter cubes and a BioSpa 8 automated incubator (BioTek). Brightfield (objective: 10×, LED intensity: 10, integration time: 13 ms, camera gain: 24) and RFP channel images (ex.: 531 nm, em.: 593 nm, LED intensity: 10, integration time: 50 ms, camera gain: 24) were taken every 2 h over a period of 26 h. About 30 min before the 26 h measurement, the plate was removed from the BioSpa 8 device and 1 µg/mL Hoechst 33,342 (ThermoFisher Scientific) was added *via* a Tecan D300e digital dispenser for an additional 26 h endpoint DAPI image. Images were processed by the BioTek gen5 data analysis software. The sum of the integrated pHAb dye fluorescence intensities of each image was normalized to the number of cells determined in the DAPI channel and subtracted by the sum of the integrated RFP signal at 0 h (background signal). The cell number and background normalized intensities were divided by the pHAb-dye DOL^F of each construct and plotted against the time. Normalized data was fitted by linear regression in GraphPad Prism (GraphPad Software, Inc.) and intracellular accumulation rates (slopes) were derived. Finally, the relative intracellular accumulation was calculated for each construct with respect to the highest intracellular accumulation rate (here, C-IgG-pHAb on MDA-MB-468 was set 100%).

FcRn and EGFR binding

Kinetic parameters of Fcabs, Cetuximab variants and their respective MMAE conjugates were determined by BLI using the Octet® RED96 system (FortéBio, Pall) at 30 °C and 1000 rpm agitation speed.

For EGFR binding analysis, Fcab variants (10 µg/mL in DPBS), C-IgG (2.5 µg/mL in DPBS) and respective MMAE conjugates were loaded onto anti-human IgG Fc capture biosensors (AHC) for 60–180 s. C-Fab (2.5 µg/mL in DPBS) was loaded onto anti-human Fab-CH1 second Generation biosensors (FAB2G) for 180 s. Biosensors were then transferred into kinetics buffer (DPBS pH 7.4, 0.02% Tween-20 and 0.1% bovine serum albumin) and incubated for 60 s followed by an association step to EGFR-His_6 (produced in-house). EGFR-His_6 was serially diluted in kinetics buffer in a concentration range varying from 20 to 0.313 nM. Association was monitored for 180, 240 or 300 s followed by a dissociation step in kinetics buffer for 600 s to determine k_{on} and k_{off} values. EGFR-His_6 was replaced by kinetics buffer, serving as a negative control and reference. Respective non-binding huFc was

used as negative control in each experiment. The buffer reference measurement (control curve) was subtracted from antibody measurements for data fitting and kinetics parameter were determined by using FortéBio data analysis software 12.0 applying a 1:1 global full-fit binding model after Savitzky-Golay filtering.

The FcRn binding assay was performed as described elsewhere (Jäger et al. 2021).

Serum stability

The serum stability assay was conducted as previously described (Dickgiesser et al. 2020) applying some minor modifications: MMAE conjugates were incubated at a final concentrations of 5 µM conjugated MMAE (considering the DAR of each construct) in human and mouse serum. Moreover, serum samples were supplemented with 5 µM deuterated D8-MMAE internal standard prior to 96 h serum incubation.

Cell proliferation assay

For the evaluation of C-IgG-, C-Fab- and Fcab-MMAE conjugates and related compounds, 40 µL of viable cell suspension were seeded into opaque 384-well plates (MDA-MB-468: 2500 cells/well, A431: 9000 cells/well, MCF-7: 5000 cells/well) followed by incubation (37 °C, 5% CO_2) in a humid chamber overnight. Test compounds were added using a D300e digital dispenser (Tecan). Free MMAE, and protein/protein-conjugate solutions were supplemented with 0.3% Tween-20 (final) and diluted to 6 µM (MMAE) or 10 µM (proteins). All wells were normalized to the maximum amount of Tween-20 added. Cell viability was determined after four days using Cell Titer Glo reagent (Promega) according to the manufacturer's instructions. Luminescence values were normalized to luminescence of non-treated cells and dose-response was fitted using the asymmetric (five parameter) fitting function of GraphPad Prism (GraphPad Software, Inc.) to derive IC_{50} values.

Results and discussion

Preparation of Fcabs, controls and pHAb-dye labeled constructs

As a starting point, we selected three different EGFR-binding Fcabs (Fcab-1, Fcab-2, Fcab-3) from literature. For all three, single-digit nanomolar binding affinities to EGFR have been described (K_D 0.7–2.6 nM) (Tuna et al. 2018). Fcabs were modified by removing the core hinge region (TCPPCP). As a negative control, we included an unmodified human Fc (huFc) fragment. As EGFR-binding references, a Cetuximab-based full length IgG (C-IgG) and a Cetuximab-derived Fab (C-Fab) fragment, both equipped with a sortase A (SrtA) recognition motif (LPETG) at the C-terminal end of the light chain, were included. Fcabs and huFc were expressed with a D265A mutation (Baudino et al. 2008; Shields et al. 2001) to avoid Fcγ receptor (I, II, III) mediated cytotoxicity (Mahalingaiah et al. 2019) and purified by affinity chromatography (Figure S1). Mass spectrometry analysis (LC-MS, Figure S2) confirmed the identity of all molecules. Differential scanning fluorimetry showed lower unfolding transition midpoints (T_m) for Fcabs (e.g. $T_{m,1}$ 59 *vs.* 66 °C; Figure S3) indicating diminished but still acceptable thermal stability of Fcabs compared to huFc. Moreover, we evaluated functional and selective cellular binding of the purified constructs (Figures S4 and S5). For cellular uptake studies all constructs were labeled at random lysines *via* amine-coupling with a fluorescent dye (pHAb-dye) (Figure 1C) that exhibits very low fluorescence at the neutral pH outside cells but strongly increased fluorescence at the acidic pH in endosomal and lysosomal compartments (Figure S6) (Nath et al. 2016). Successful pHAb-dye labeling and the absence of aggregates were confirmed by analytical size exclusion chromatography (SE-HPLC) (Figure S8). To ensure comparability between individual fluorescence intensities resulting from differently labeled constructs, the fluorescence signals were normalized. A comprehensive description of the underlying experimental procedures can be found in the Supporting Information (SI).

Cellular uptake studies

To assess the general suitability of EGFR-binding Fcabs for intracellular drug delivery, their uptake and accumulation into cancer cells were studied. Therefore, pHAb-dye labeled constructs were incubated on EGFR overexpressing (MDA-MB-468, A431) and EGFR negative (MCF-7) adherent cells and fluorescence was continuously measured over 26 h (Figure S9A). Fluorescence intensities were normalized to account for individual cell numbers and fluorescence intensities of labelled constructs. These intensities were plotted against the time to determine intracellular accumulation rates by linear regression (Figure S9B). All accumulation rates were expressed relative to the rate of C-IgG-pHAb (C-IgG-pHAb on MDA-MB-468) which showed the fastest uptake (Figure 2). Differences in accumulation between MDA-MB-468 and A431 cells directly correlated with the differences in specific EGFR expression density. Remarkably, all Fcabs underwent selective, EGFR-mediated cellular uptake. Interestingly, bivalent and monovalent controls C-IgG-pHAb and C-Fab-pHAb exhibited most pronounced internalization, which may arise from different epitopes addressed by Cetuximab than by the Fcabs (Tuna et al. 2018). To measure the therapeutic threshold (IC_{50}) for respective Fcab-drug conjugates, Fcabs were conjugated to cytotoxic payloads and tested for their cell killing activity.

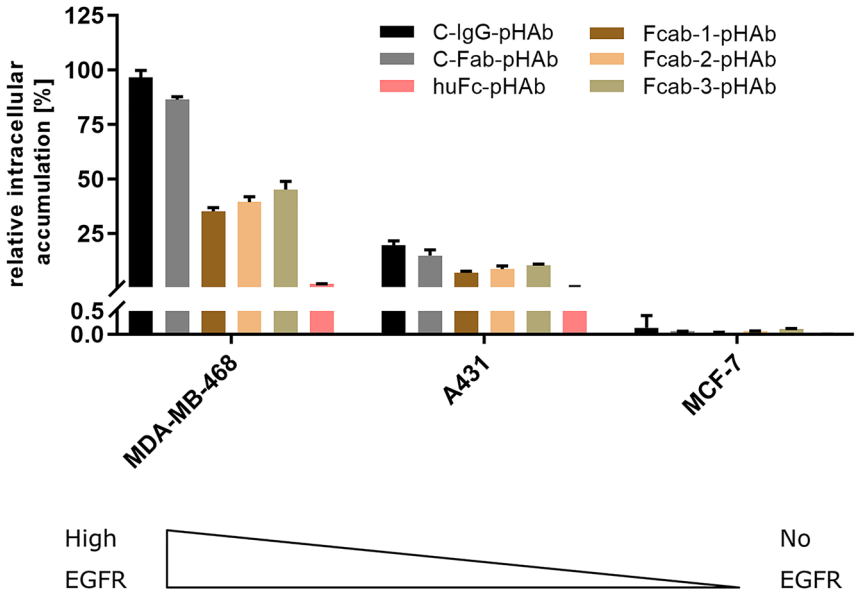

Figure 2: Intracellular accumulation of Fcab-, huFc-, C-Fab- and C-IgG-pHAb dye conjugates relative to the accumulation rate of C-IgG-pHAb on MDA-MB-468 cells (100%).
Intracellular accumulation rates were derived from 0 to 26 h incubation at 100 nM and normalized to cell number and individual pHAb-dye fluorescence of each construct. Relative EGFR expression profiles (MDA-MB-468 > A431 > MCF-7) are indicated below bar graph. Error bars show the standard deviation of triplicates.

Generation of Fcab-drug conjugates

Fcab-1, Fcab-2, Fcab-3 and huFc were conjugated by an engineered microbial transglutaminase (mTG) (Dickgiesser et al. 2020) targeting Q295 with Val-Cit-PAB-MMAE possessing a triple glycine handle (**1**) (Figure 3) (Table 1) and purified by preparative size exclusion chromatography (Figure S10). C-Fab and C-IgG were conjugated to **1** by SrtA (Chen et al. 2011; Gébleux et al. 2019) reaching DARs ranging DAR 0.8–1.1. Analytical SE-HPLC of purified conjugates showed the absence of high molecular weight species (Figure S11A) (Table 1). Surprisingly, analyses *via* reversed phase chromatography (RP-HPLC) (Figure S11B), hydrophobic interaction chromatography (HI-HPLC) (Table S2) and LC-MS (Figure S12) revealed that all three Fcabs showed an elevated DAR between 2.7 and 2.9. This was not observed for huFc (DAR 2.0) indicating that substrate **1** had been coupled to additional residues in the Fcab scaffold only (Table 1). The additional conjugation sites could subsequently be identified *via* LC-MS peptide mapping as Q311 and Q438 in the constant C_H2 and C_H3 region (Figures 3A and 4). The disappearance of peaks assigned to unconjugated peptides containing Q295 in the digested Fcab-1-MMAE mixture (Figure 4; peak a, b) indicated that Fcabs were nearly completely conjugated at position Q295 while only partially conjugated at position Q311 and Q438 (total 18–23% conjugated based on DAR 2.7–2.9). As previous mTG conjugation to the same constant region in HER2 Fcabs or native IgGs did not lead to Q311 or Q438 conjugation (Dickgiesser et al. 2020; Jäger et al. 2021), accessibility for mTG and altered conjugation has most likely been driven by structural changes or electrostatic effects in adjacent regions. These changes must be induced by the EGFR paratope inserted to the C_H3 region or by the missing core hinge region of the EGFR Fcabs. All three conjugation positions, namely Q295, Q311 and Q438 lie within the solvent exposed exterior of the Fcab. Consequently, conjugation could theoretically affect accessibility for serum proteases and interfere with FcRn and EGFR binding. To assess this notion, Fcab-1-MMAE, Fcab-2-MMAE and Fcab-3-MMAE were subsequently tested for FcRn and EGFR binding and serum stability.

Receptor binding properties of Fcab-drug conjugates

Fcab-MMAE conjugates were analyzed along with controls and non-conjugated parent molecules for their binding affinity to the target receptor EGFR and half-life extending FcRn (Table 2) (Figure S13) (Tables S3 and S4). Biolayer interferometry (BLI) measurements did not reveal impaired binding (K_D) of conjugates to EGFR and FcRn with differences in K_D beyond the assay variability

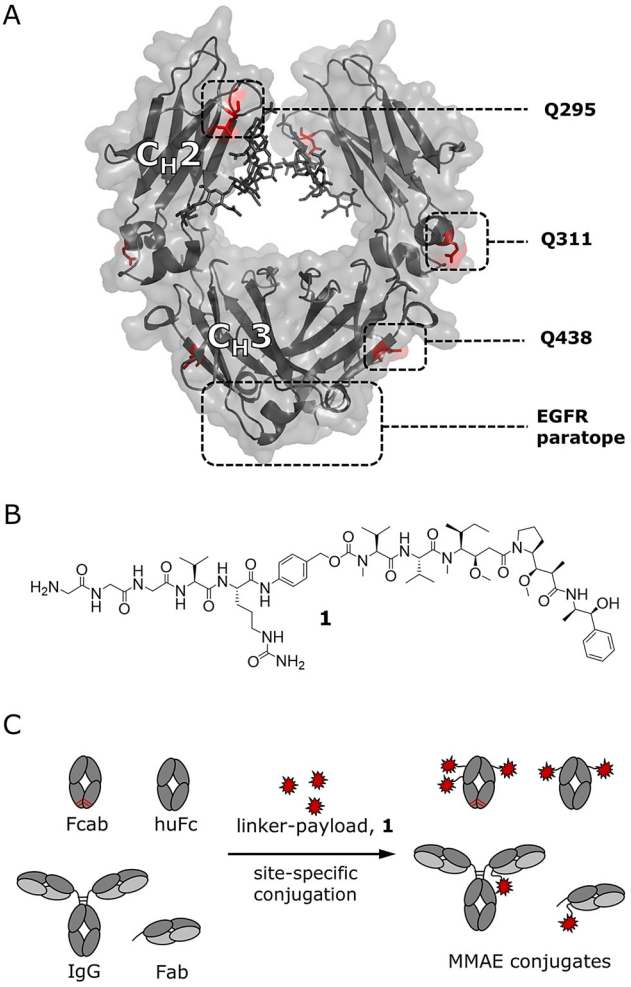

Figure 3: Fcab-drug conjugates.
(A) Representative figure of a human Fc portion (PDB ID 5VGP) showing the EGFR binding site located in the C_H3 region as well as the conjugation sites Q295, Q311 and Q438 (EU numbering). (B) Structure of linker-payload **1**. (C) Schematic representation of MMAE conjugation.

(twofold) suggesting that attached payloads at positions Q295 do not impact binding functionalities of both receptors. However, for Q311 and Q438 it should be noted that effects on EGFR and FcRn binding cannot be assessed robustly with our BLI assay because of just minor conjugation (18–23%).

Serum stability of Fcab-drug-conjugates

Several studies have shown, that conjugate pharmacokinetics can strongly be influenced by premature cleavage of the linker that connects the protein with the cytotoxic drug (Dorywalska et al. 2015; Shen et al. 2012; Strop et al. 2013). The Val-Cit linker motif is especially prone to cleavage by a carboxylesterase (mCes1c) that is present in mouse serum but absent in human serum (Dorywalska et al. 2016). The extend of this instability heavily depends on the chosen conjugation sites. When Fcab-MMAE conjugates were incubated in mouse and human serum for 96 h, no free MMAE could be detected for all constructs. This indicates that the Val-Cit linker motif is not accessible for mCes1c neither at position Q295 nor at the novel positions Q311 and Q438, hence all positions protect the conjugate from being cleaved prematurely (Table 2).

Table 1: Overview of conjugated Fcabs and controls.

		Conjugation			
Conjugate	**Size [kDa]**	**Site**	**Technique**	**DAR**	**SE-HPLC purity [%]**
Fcab-1-MMAE	52.02	Q295, Q311, Q438	mTG	2.9	96.7
Fcab-2-MMAE	51.07	Q295, Q311, Q438	mTG	2.7	98.5
Fcab-3-MMAE	51.93	Q295, Q311, Q438	mTG	2.8	99.7
huFc-MMAE	53.00	Q295	mTG	2.0	100.0
C-Fab-MMAE	50.49	LC-*C*-LPETG	SrtA	0.8	99.5
C-IgG-MMAE	155.37	LC-*C*-LPETG	SrtA	1.1	99.5

Size refers to unconjugated protein including the most abundant glycosylation pattern as measured by LC-MS. DAR is given as a mean from RP-HPLC and LC-MS analysis. SE-HPLC purity refers to the final drug conjugate and was analyzed after a freeze-thaw cycle. LC-*C* – light chain C-terminus.

In vitro cytotoxicity of Fcab-drug conjugates

Next, we evaluated selective cell killing capabilities of the Fcab-drug conjugates in an *in vitro* cell proliferation assay (Figure 5). All Fcab-drug conjugates showed similar subnanomolar inhibitory activity on EGFR positive MDA-MB-468 and A431 cells (IC_{50} 0.18–0.22 nM and 0.23–0.32 nM, respectively) while toxicity against EGFR negative MCF-7 cells was decreased by several orders of magnitude (IC_{50} > 100 nM) indicating strong target-dependent cell killing. Non-targeting huFc-MMAE showed low toxicity as well (MDA-MB-468: IC_{50} > 300 nM; A431 and MCF-7: IC_{50} > 100 nM) confirming that Fcab-MMAE toxicity is primarily driven by specific receptor-mediated uptake. In line with higher cellular uptake on MDA-MB-468 cells compared to A431 cells (Figure 2), Fcab-drug conjugates and Cetuximab controls showed higher activity on MDA-MB-468 cells compared to A431 (Figure 5B). Furthermore, higher potency

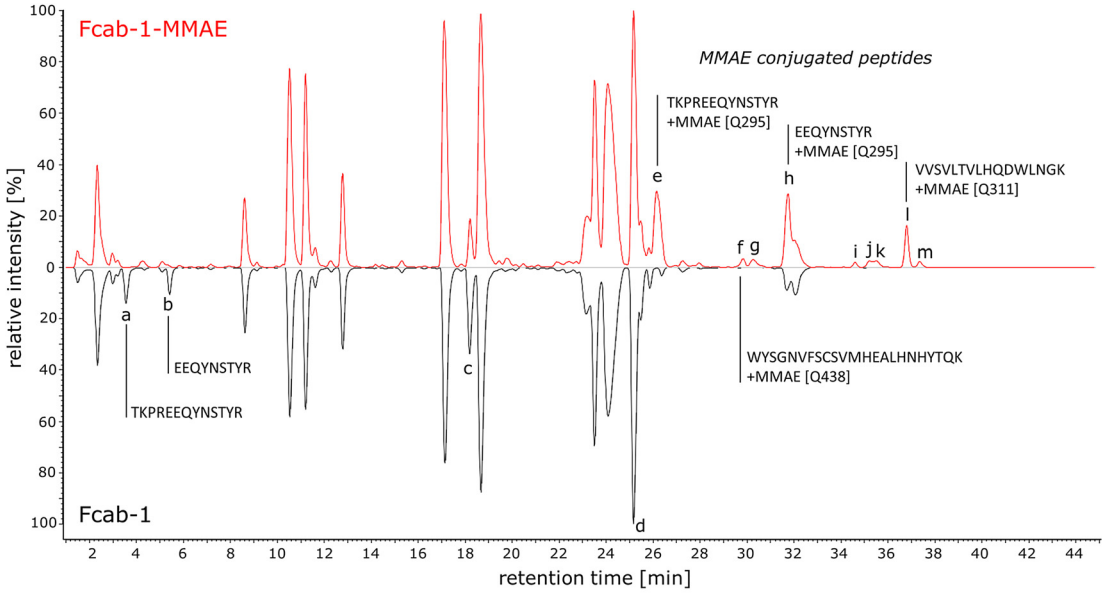

peak	t_R [min]	peptide	modification	calculated mass [Da]	m/z	Δmass [Da]
a	3.61	TKPREEQYNSTYR	-	1670.80	557.94	0.00
b	5.47	EEQYNSTYR	GlcNAc-Fuc [N297]	1537.64	769.83	0.00
c	18.31	WYSGNVFSCSVMHEALHNHYTQK	carbamidomethyl [C425]	2794.24	699.57	0.01
d	25.35	VVSVLTVLHQDWLNGK	-	1807.00	603.35	0.01
e	26.33	TKPREEQYNSTYR	MMAE [Q295]	3297.53	825.19	0.80
f	30.00	WYSGNVFSCSVMHEALHNHYTQK	carbamidomethyl [C425], MMAE [Q438]	4071.83	1018.77	0.78
g	30.46	FNWYVDGVEVHNAKTKPREEQYNSTYR	G2FSA2 glycan [N297], MMAE [Q295]	6958.01	994.37	4.50
h	31.92	EEQYNSTYR	MMAE [Q295], GlcNAc-Fuc [N297]	2815.24	1408.23	0.79
i	34.79	VVSVLTVLHQDWLNGKEYK	MMAE [Q311]	3504.79	1169.00	0.79
j	35.38	APELLGGPSVFLFPPKPKDTLMISR	oxidated [M252]	2725.49	682.37	0.03
k	35.57	VVSVLTVLHQDWLNGKEYK	deamidated [N315], MMAE [Q311]	3505.78	1169.34	0.79
l	36.99	VVSVLTVLHQDWLNGK	MMAE [Q311]	3084.59	1542.91	0.79
m	37.52	VVSVLTVLHQDWLNGK	deamidated [N315], MMAE [Q311]	3085.58	1029.27	0.79

Figure 4: Conjugation site identification.
LC-MS chromatogram of digested Fcab-1-MMAE shows conjugated peptides (e–i, k–m) that were not detected in the Fcab-1 preparation. Conjugated peptides eluted at higher retention times due to hydrophobic MMAE. Matched pairs of unconjugated peptides (a–d) eluted at lower retention times and peaks disappeared (a, b) or showed reduced intensity (c) in the Fcab-1-MMAE preparation compared to Fcab-1.

Table 2: Binding affinity and serum stability of Fcab-drug conjugates and controls.

	Non-conjugated		MMAE-conjugates		Free MMAE (% total MMAE)	
Conjugate	**K_D (EGFR) [nM]**	**K_D (FcRn) [nM]**	**K_D (EGFR) [nM]**	**K_D (FcRn) [nM]**	**Mouse**	**Human**
Fcab-1-MMAE	2.42 ± 0.01	381 ± 12	2.67 ± 0.02	309 ± 10	1.3	0.3
Fcab-2-MMAE	1.07 ± 0.01	329 ± 13	1.37 ± 0.01	362 ± 12	1.1	0.0
Fcab-3-MMAE	1.71 ± 0.01	589 ± 22	1.54 ± 0.01	337 ± 12	0.9	0.0
huFc-MMAE	0.0	n.d.	0.0	n.d.	n.d.	n.d.
C-Fab-MMAE	0.82 ± 0.01	–	n.d.	–	n.d.	n.d.
C-IgG-MMAE	1.25 ± 0.01	747 ± 24	0.60 ± 0.01	892 ± 31	n.d.	n.d.

Dissociation constants (K_D) were measured by BLI. Binding to recombinantly produced EGFR and FcRn were measured at pH 7.4 and 6.0, respectively. Errors are standard errors from fitting using FortéBio data analysis software 12.0. Twofold changes of K_D are in the range of assay variability. Free MMAE was measured *via* LC-MS/MS after incubation in mouse and human sera at 37 °C for 96 h (n = 3). Numbers show the released fraction relative to initially conjugated MMAE. n.d. – not determined.

A

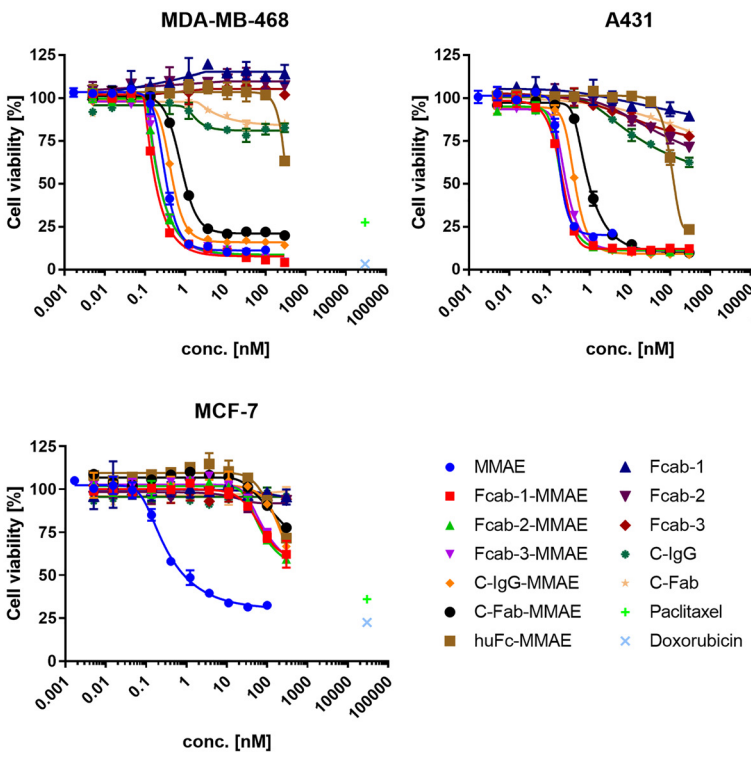

B

	IC_{50} [nM]		
conjugate	MDA-MB-468	A431	MCF-7
Fcab-1-MMAE	0.18 ± 0.03	0.23 ± 0.04	> 100
Fcab-2-MMAE	0.19 ± 0.05	0.27 ± 0.07	> 100
Fcab-3-MMAE	0.22 ± 0.01	0.32 ± 0.08	> 100
huFc-MMAE	> 300	> 100	> 100
C-Fab-MMAE	0.78 ± 0.03	0.99 ± 0.29	> 100
C-IgG-MMAE	0.44 ± 0.03	0.50 ± 0.08	> 100
MMAE	0.32 ± 0.03	0.17 ± 0.01	0.34 ± 0.10

Figure 5: Cell proliferation assays.
(A) Cell viability on EGFR positive (MDA-MB-468, A431) and EGFR negative cells (MCF-7). Cells were incubated with serial dilution of MMAE conjugates and free MMAE for 4 days before cell viability was analyzed. Error bars represent standard deviation (SD) of triplicates (B) Inhibitory activity of MMAE conjugates and free MMAE. IC_{50} values are given as mean of three independent experiments (IC_{50} ± SD).

of Fcab-drug conjugates on EGFR positive cells (IC_{50} 0.18–0.32 nM) compared to C-Fab-MMAE (IC_{50} 0.78–0.99 nM) or C-IgG-MMAE (IC_{50} 0.44–0.50 nM) suggested that reduced intracellular accumulation of Fcabs (Figure 2) may be compensated by their higher DAR enabled by additional conjugation to Q311 and Q438 (2.7–2.9 *vs.* 0.8 and 1.1, respectively). Overall, the results indicate that *in vitro* potency of Fcab-drug conjugates is in the typical subnanomolar range of ADCs despite their monovalent binding mode.

Conclusion

We have recently demonstrated the suitability of the Fcab format for generation of drug conjugates using HER2 binding Fcabs in a first feasibility study (Jäger et al. 2021). Here, we have further expanded the concept of Fcab-drug conjugates to constructs that carry a higher drug load and are targeted against the therapeutically relevant solid cancer target EGFR. Fcabs produced in the scope of this study bound EGFR with nanomolar affinity and accumulated

target-dependently in EGFR expressing cells. Site-specific conjugation to Q295 and the novel positions Q311 and Q438 *via* mTG yielded DAR 2.7–2.9 Val-Cit-PAB-MMAE conjugates without altered EGFR or FcRn binding affinities. Generated Fcab-drug conjugates exhibited high stability in human and mouse serum and showed EGFR-mediated cytotoxicity at sub-nanomolar concentrations similar to Cetuximab-based reference conjugates. The Fcab-drug conjugate candidates presented herein show favorable stability and potency profiles suggesting further animal studies to evaluate whether Fcabs' smaller size and intermediate plasma half-life are beneficial for ADC exposure to solid tumors.

Acknowledgements: The authors thank L. Basset for bioconjugation and analytics; S. Keller, A. Müller, C. Brunori and D. Müller-Pompalla for advice and laboratory support in protein purification; J. Schanz and R. Kellner for LC-MS measurements; J. Roßkopf for reference constructs; the manuscript anonymous reviewers for comments and suggestions.

Author contributions: All the authors have accepted responsibility for the entire content of this submitted manuscript and approved submission.

Research funding: None declared.

Conflict of interest statement: The authors declare no conflicts of interest regarding this article.

References

Aubrey, N., Allard-Vannier, E., Martin, C., Bryden, F., Letast, S., Colas, C., Lakhrif, Z., Collinet, N., Dimier-Poisson, I., Chourpa, I., et al. (2018). Site-specific conjugation of auristatins onto engineered scFv using second generation maleimide to target HER2-positive breast cancer *in vitro*. Bioconjugate Chem. 29: 3516–3521.

Baudino, L., Shinohara, Y., Nimmerjahn, F., Furukawa, J., Nakata, M., Martínez-Soria, E., Petry, F., Ravetch, J.V., Nishimura, S., and Izui, S. (2008). Crucial role of aspartic acid at position 265 in the CH2 domain for murine IgG2a and IgG2b Fc-associated effector functions. J. Immunol. 181: 6664–6669.

Boni, V., Sharma, M.R., and Patnaik, A. (2020). The resurgence of antibody drug conjugates in cancer therapeutics: novel targets and payloads. Am. Soc. Clin. Oncol. Educ. Book 40: e58–e74.

Cao, L., Li, Q., Tong, Z., Xing, Y., Xu, K., Yijia Wang, J., Li, W., Zhao, J., Zhao, L., and Hong, Z. (2020). HER2-specific immunotoxins constructed based on single-domain antibodies and the improved toxin PE24X7. Int. J. Pharm. 574: 118939.

Chen, I., Dorr, B.M., and Liu, D.R. (2011). A general strategy for the evolution of bond-forming enzymes using yeast display. Proc. Natl. Acad. Sci. U. S. A. 108: 11399–11404.

Deonarain, M.P. (2018). Miniaturised 'antibody'-drug conjugates for solid tumours? Drug Discov. Today Technol. 30: 47–53.

Dickgiesser, S., Rieker, M., Mueller-Pompalla, D., Schröter, C., Tonillo, J., Warszawski, S., Raab-Westphal, S., Kühn, S., Knehans, T., Könning, D., et al. (2020). Site-specific conjugation of native antibodies using engineered microbial transglutaminases. Bioconjugate Chem. 31: 1070–1076.

Dorywalska, M., Dushin, R., Moine, L., Farias, S.E., Zhou, D., Navaratnam, T., Lui, V., Hasa-Moreno, A., Casas, M.G., Tran, T.-T., et al. (2016). Molecular basis of valine-citrulline-PABC linker instability in site-specific ADCs and its mitigation by linker design. Mol. Canc. Therapeut. 15: 958–970.

Dorywalska, M., Strop, P., Melton-Witt, J.A., Hasa-Moreno, A., Farias, S.E., Galindo Casas, M., Delaria, K., Lui, V., Poulsen, K., Loo, C., et al. (2015). Effect of attachment site on stability of cleavable antibody drug conjugates. Bioconjugate Chem. 26: 650–659.

Gébleux, R., Briendl, M., Grawunder, U., and Beerli, R.R. (2019). Sortase A enzyme-mediated generation of site-specifically conjugated antibody–drug conjugates. In: Nuijens, T. and Schmidt, M. (Eds.), *Enzyme-mediated ligation methods. Methods in molecular biology*. Humana, New York, pp. 1–13.

Glassman, P.M., Walsh, L.R., Villa, C.H., Marcos-Contreras, O.A., Hood, E.D., Muzykantov, V.R., and Greineder, C.F. (2020). Molecularly engineered nanobodies for tunable pharmacokinetics and drug delivery. Bioconjugate Chem. 31: 1144–1155.

Higgins, J.P., Sarkar, A., Williams, E.T., Iberg, A., Waltzman, R., and Willert, E.K. (2020). Abstract P1-18-35: MT-5111, a novel HER2 targeting engineered toxin body, under clinical development to overcome mechanisms of resistance to existing HER2 targeted therapies. *Poster Sess. Abstr.* Canc. Res. 80: P1-18–35.

Jäger, S., Wagner, T.R., Rasche, N., Kolmar, H., Hecht, S., and Schröter, C. (2021). Generation and biological evaluation of Fc antigen binding fragment-drug conjugates as a novel antibody-based format for targeted drug delivery. Bioconjugate Chem. 32: 1699–1710.

Khongorzul, P., Ling, C.J., Khan, F.U., Ihsan, A.U., and Zhang, J. (2020). Antibody-drug conjugates: a comprehensive review. Mol. Canc. Res. 18: 3–19.

Leung, K.M., Batey, S., Rowlands, R., Isaac, S.J., Jones, P., Drewett, V., Carvalho, J., Gaspar, M., Weller, S., Medcalf, M., et al. (2015). A HER2-specific modified Fc fragment (Fcab) induces antitumor effects through degradation of HER2 and apoptosis. Mol. Ther. 23: 1722–1733.

Li, Q., Barrett, A., Vijayakrishnan, B., Tiberghien, A., Beard, R., Rickert, K.W., Allen, K.L., Christie, R.J., Marelli, M., Harper, J., et al. (2019). Improved inhibition of tumor growth by diabody-drug conjugates via half-life extension. Bioconjugate Chem. 30: 1232–1243.

Li, Z., Li, Y., Chang, H.P., Chang, H.Y., Guo, L., and Shah, D.K. (2019). Effect of size on solid tumor disposition of protein therapeutics. Drug Metab. Dispos. 47: 1136–1145.

Liu, W., Zhao, W., Bai, X., Jin, S., Li, Y., Qiu, C., Pan, L., Ding, D., Xu, Y., Zhou, Z., et al. (2019). High antitumor activity of Sortase A-generated anti-CD20 antibody fragment drug conjugates. Eur. J. Pharmaceut. Sci. 134: 81–92.

Lobner, E., Traxlmayr, M.W., Obinger, C., and Hasenhindl, C. (2016). Engineered IgG1-Fc – one fragment to bind them all. Immunol. Rev. 270: 113–131.

Mahalingaiah, P.K., Ciurlionis, R., Durbin, K.R., Yeager, R.L., Philip, B.K., Bawa, B., Mantena, S.R., Enright, B.P., Liguori, M.J., and Van Vleet, T.R. (2019). Potential mechanisms of target-independent uptake and toxicity of antibody-drug conjugates. Pharmacol. Ther. 200: 110–125.

Mullard, A. (2020). FDA approves first BCMA-targeted therapeutic. Nat. Rev. Drug Discov. 19: 659.

Mullard, A. (2021). FDA approves ADC therapeutics' loncastuximab tesirine, ushering in a new cytotoxic payload. Nat. Rev. Drug Discov. 20: 414.

Nath, N., Godat, B., Zimprich, C., Dwight, S.J., Corona, C., McDougall, M., and Urh, M. (2016). Homogeneous plate based antibody internalization assay using pH sensor fluorescent dye. J. Immunol. Methods 431: 11–21.

Nessler, I., Khera, E., Vance, S., Kopp, A., Qiu, Q., Keating, T.A., Abu-Yousif, A.O., Sandal, T., Legg, J., Thompson, L., et al. (2020). Increased tumor penetration of single-domain antibody-drug conjugates improves *in vivo* efficacy in prostate cancer models. Canc. Res. 80: 1268–1278.

Ruddle, B.T., Fleming, R., Wu, H., Gao, C., and Dimasi, N. (2019). Characterization of disulfide bond rebridged Fab–drug conjugates prepared using a dual maleimide pyrrolobenzodiazepine cytotoxic payload. ChemMedChem 14: 1185–1195.

Shen, B., Xu, K., Liu, L., Raab, H., Bhakta, S., Kenrick, M., Parsons-Reponte, K.L., Tien, J., Yu, S., Mai, E., et al. (2012). Conjugation site modulates the *in vivo* stability and therapeutic activity of antibody-drug conjugates. Nat. Biotechnol. 30: 184–189.

Shields, R.L., Namenuk, A.K., Hong, K., Meng, Y.G., Rae, J., Briggs, J., Xie, D., Lai, J., Stadlen, A., Li, B., et al. (2001). High resolution mapping of the binding site on human IgG1 for FcγRI, FcγRII, FcγRIII, and FcRn and design of IgG1 variants with improved binding to the FcγR. J. Biol. Chem. 276: 6591–6604.

Strop, P., Liu, S., Dorywalska, M., Delaria, K., Dushin, R.G., Tran, T., Ho, W., Farias, S., Casas, M.G., Abdiche, Y., et al. (2013). Location matters: site of conjugation modulates stability and pharmacokinetics of antibody drug conjugates. Chem. Biol. 20: 161–167.

Syed, Y.Y. (2020). Sacituzumab govitecan: first approval. Drugs 80: 1019–1025.

Thurber, G.M., Schmidt, M.M., and Wittrup, K.D. (2008). Antibody tumor penetration: transport opposed by systemic and antigen-mediated clearance. Adv. Drug Deliv. Rev. 60: 1421–1434.

Tuna, M., Leung, K.-M., Sun, H., Medcalf, M., and Isaac, S. (2018). EGFR binding molecules. CA3030505A1.

Wozniak-Knopp, G., Bartl, S., Bauer, A., Mostageer, M., Woisetschläger, M., Antes, B., Ettl, K., Kainer, M., Weberhofer, G., Wiederkum, S., et al. (2010). Introducing antigen-binding sites in structural loops of immunoglobulin constant domains: Fc fragments with engineered HER2/neu-binding sites and antibody properties. Protein Eng. Des. Sel. 23: 289–297.

Supplementary Material: The online version of this article offers supplementary material (https://doi.org/10.1515/hsz-2021-0321).